

## High-Resolution Ozone Imager (HIROIG) Final Report

10 January 1998

Prepared by

D. L. MCKENZIE, K. B. CRAWFORD, D. J. GUTIERREZ,  
J. H. HECHT, N. KATZ, D. J. MABRY, and W. J. SKINNER  
Space and Environment Technology Center  
Technology Operations

Prepared for

SPACE AND MISSILE SYSTEMS CENTER  
AIR FORCE MATERIEL COMMAND  
2430 E. El Segundo Boulevard  
Los Angeles Air Force Base, CA 90245

19990511 063

Corporate Business Division

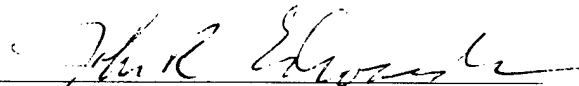
APPROVED FOR PUBLIC RELEASE;  
DISTRIBUTION UNLIMITED

DTIC QUALITY INSPECTED 4

This report was submitted by The Aerospace Corporation, El Segundo, CA 90245-4691, under Contract No. F04701-93-C-0094 with the Space and Missile Systems Center, 2430.E. El Segundo Blvd., Los Angeles Air Force Base, CA 90245. It was reviewed and approved for The Aerospace Corporation by A. B. Christensen Principal Director, Space and Environment Technology Center. J. R. Edwards was the project officer for the program.

This report has been reviewed by the Public Affairs Office (PAS) and is releasable to the National Technical Information Service (NTIS). At NTIS, it will be available to the general public, including foreign nationals.

This technical report has been reviewed and is approved for publication. Publication of this report does not constitute Air Force approval of the report's findings or conclusions. It is published only for the exchange and stimulation of ideas.

  
J. R. EDWARDS  
SMC/AXVF

**REPORT DOCUMENTATION PAGE**Form Approved  
OMB No. 0704-0188

Public reporting burden for this collection of information is estimated to average 1 hour per response, including the time for reviewing instructions, searching existing data sources, gathering and maintaining the data needed, and completing and reviewing the collection of information. Send comments regarding this burden estimate or any other aspect of this collection of information, including suggestions for reducing this burden to Washington Headquarters Services, Directorate for Information Operations and Reports, 1215 Jefferson Davis Highway, Suite 1204, Arlington, VA 22202-4302, and to the Office of Management and Budget, Paperwork Reduction Project (0704-0188), Washington, DC 20503.

1. AGENCY USE ONLY (Leave blank)		2. REPORT DATE 10 January 1998		3. REPORT TYPE AND DATES COVERED	
4. TITLE AND SUBTITLE High-Resolution Ozone Imager (HIROIG) Final Report				5. FUNDING NUMBERS  F04701-93-C-0094	
6. AUTHOR(S) D. L. McKenzie, K. B. Crawford, D. J. Gutierrez, J. H. Hecht, N. Katz, D. J. Mabry, and W. J. Skinner					
7. PERFORMING ORGANIZATION NAME(S) AND ADDRESS(ES) The Aerospace Corporation Technology Operations El Segundo, CA 90245				8. PERFORMING ORGANIZATION REPORT NUMBER  TR-98(1306)-2	
9. SPONSORING/MONITORING AGENCY NAME(S) AND ADDRESS(ES) Space and Missile Systems Center Air Force Materiel Command 2430 E. El Segundo Blvd. Los Angeles Air Force Base, CA 90245				10. SPONSORING/MONITORING AGENCY REPORT NUMBER  SMC-TR-99-13	
11. SUPPLEMENTARY NOTES					
12a. DISTRIBUTION/AVAILABILITY STATEMENT Approved for public release; distribution unlimited				12b. DISTRIBUTION CODE	
13. ABSTRACT (Maximum 200 words) The High-Resolution Ozone Imager (HIROIG) is a hyperspectral UV imaging spectrograph/polarimeter designed for space flight with the specific purpose of searching for direct evidence of stratospheric ozone depletion caused by launch-vehicle exhaust. Solid-rocket motors deposit several tons of chlorine, primarily in the form of HCl, per kilometer in the stratosphere. Theoretical analysis and simulations have suggested that a significant amount of HCl may be converted into active chlorine, which can destroy ozone. HIROIG looks for stratospheric ozone depletion by measuring the spectrum of solar UV radiation backscattered by the atmosphere. HIROIG's primary mission places several unique demands on the instrument; it has 2 km spatial resolution, continuous spectral coverage of the 270-370 nm wavelength band, and, in order to distinguish scattering by launch-plume aerosols from atmospheric Rayleigh scattering, it can completely characterize the polarization of the incident light. A measurement sequence over a launch site requires collection of approximately 40 Mbytes of data in about 2 min. A prototype instrument has been built and deployed for ground-based field operations, and an engineering model of the full instrument, including flight-quality optics, has been designed and partially assembled.					
14. SUBJECT TERMS Stratospheric ozone, Launch vehicles, UV spectroscopy/polarimetry				15. NUMBER OF PAGES  25	
				16. PRICE CODE	
17. SECURITY CLASSIFICATION OF REPORT UNCLASSIFIED	18. SECURITY CLASSIFICATION OF THIS PAGE UNCLASSIFIED	19. SECURITY CLASSIFICATION OF ABSTRACT UNCLASSIFIED		20. LIMITATION OF ABSTRACT	

## **Acknowledgment**

The authors wish to acknowledge the contributions of the following colleagues to the HIROIG program: E. R. Abendroth, W. R. Crain, C. R. Ibscher, P. H. Lew, S. H. Penzin, M. N. Ross, D. A. Roux, J. A. Stein, and P. Taubman. We wish to thank J. R. Edwards, D. Pilson, and Maj. B. Hedley of the US Air Force Space and Missile Systems Center Environmental Management Division and A. D. Abbott, T. Spiglanin, and V. Lang of The Aerospace Corporation's Environmental Programs Office for their support.

## Contents

1.	Introduction .....	1
2.	Stratospheric Ozone Depletion by Launch Vehicles .....	3
3.	The HIROIG Instrument.....	5
3.1	Optics .....	7
3.2	Detector .....	8
3.3	Data Processing Unit .....	12
3.4	Calibration .....	15
3.5	Electronic Ground Support Equipment .....	16
4.	HIROIG Instrument Development Status.....	17
5.	Ground-Based Observations.....	19
6.	Summary .....	23
	References .....	25

## Figures

1.	"Push-broom" operation of the HIROIG instrument in a Sun-synchronous polar orbit, illustrating the 100-km swath and the 2-km spatial resolution .....	5
2.	Illustration of the effects of an "ozone hole" on the backscattered solar UV radiation as viewed from space.....	6
3.	A cross-sectional view of one of the three identical spectrographs in the HIROIG flight instrument. ....	7
4.	Layout of the 1024 x 1024-pixel HIROIG CCD detectors .....	9
5.	The UV spectrum of the diffuse sky as recorded by the HIROIG prototype instrument at Kennedy Space Center on July 7, 1994 at 13:20 EDT, when the Sun was near the zenith .....	9
6.	Illustration of the modes of operation of the parallel registers of the HIROIG CCD detector.....	10

7. Block diagram of the HIROIG CCD detector electronics. ....	11
8. Block diagram of the HIROIG data processing unit.....	13
9. Block diagram of the HIROIG solid-state data recorder. ....	14
10. Plot of the intensity ratio of diffuse sky radiation in bands centered on 299.9 nm and 297.7 nm as a function of time on July 8, 1994.....	20
11. Comparison of the change in total column ozone inferred from the HIROIG UV spectra with that predicted by an empirical model, for July 8, 1994, following the STS-65 launch.....	21

## 1. Introduction

Ozone ( $O_3$ ) in the stratosphere plays a vital role in sustaining life on the Earth's surface by absorbing solar ultraviolet (UV) radiation. Depletion of the stratospheric ozone layer has consequences extending from sunburn to increased risk of cancer. Because of this, international treaties and protocols have the goal of completely eliminating the use of ozone-depleting substances and, thus, slowing and eventually halting the further destruction of the stratospheric ozone layer.

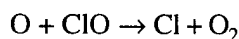
All Government programs are mandated by the National Environmental Policy Act (NEPA) to consider the adverse environmental effects of their activities. Programs are required to assess the environmental impacts of their activities and to report the results of the assessment to the public.

Operational military space programs depend heavily on solid rocket motors (SRMs) for heavy lift capability, especially the Titan IV, and to a lesser extent, the space shuttle. Solid rocket motors using ammonium perchlorate as an oxidizer deposit large quantities of chlorine, in the form of hydrogen chloride (HCl), and aerosols ( $Al_2O_3$  or "alumina") in the stratosphere. HCl is converted into active chlorine, which catalyzes the destruction of stratospheric ozone. The alumina particles may also play a role in ozone destruction by providing a site for chemical reactions. Rocket launches are thought to play a minor role in global ozone depletion, but transient local ozone destruction caused by reactions in the launch-plume remnant may approach 100% and last for several hours. The risk to organisms on the ground may be mitigated by dispersal of the plume remnant in the stratosphere so that the *total column ozone* depletion along a line of sight from a point on the ground to the Sun remains small. The total ozone column is the determiner of how much UV radiation is absorbed and is, thus, the parameter of greatest importance.

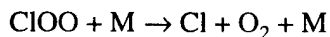
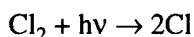
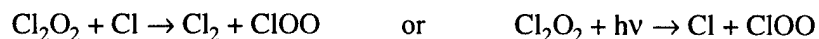
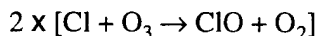
The Environmental Management Division of the Air Force Space and Missile Systems Center (SMC) has embarked upon an integrated program of observations, laboratory work, modeling, and theory to assess the local impact of solid-rocket launches on the stratospheric ozone layer. The High-Resolution Ozone Imager (HIROIG) was conceived to be the spaceborne component of this program. The instrument makes measurements of the spectrum of solar UV radiation backscattered by the Earth's atmosphere. From these measurements, stratospheric ozone densities can be inferred. Remote measurements from space are a critical component of the program because other techniques sample only small regions and thus may not look in the right place at the right time. Earth-based measurements may also be adversely affected by weather or may be denied access to certain launch sites. On the other hand, to be effective, a spaceborne instrument must make measurements in sunlight within a few hours after launch. This requirement results in only a fraction of launches being observable from space. However, the instrument sensitivity and field of view are such that the absence of measurable change in the ultraviolet spectrum will assure that the biological effects of ozone depletion by a launch are negligible.

## 2. Stratospheric Ozone Depletion by Launch Vehicles

Solid-fuel rocket motors (SRMs) deposit several tons of chlorine per kilometer, primarily in the form of HCl, into the atmosphere below their burn-out altitude of approximately 40 km (Ross 1996). Computer simulations and theoretical work have suggested that significant amounts of HCl are converted to the active species Cl and Cl<sub>2</sub> by afterburning reactions in rocket motor plumes (Zittel 1994; Denison, *et al.* 1994). In the presence of sunlight, which is the only condition under which the transient destruction of ozone would be important, photolysis converts Cl<sub>2</sub> to Cl on a time scale that is short compared to an hour. Free Cl can then destroy ozone catalytically by:



At low altitudes, where the pressure of a third species M is significant, the catalytic *ClO dimer* mechanism, which plays an important role in the formation of the south polar ozone hole, may also be effective in rocket plumes. That is,



This mechanism was proposed by L. R. Martin and his colleagues (Martin 1994; Brady and Martin 1995). In the case of a Titan IV launch, reaction (1) could produce a region totally devoid of stratospheric ozone that has a diameter of order 1–2 km (Ross *et al.* 1997), but the catalytic ClO dimer mechanism might produce an ozone hole many times larger.



Even if deep ozone depletion caused by the ClO dimer mechanism occurs, it will not necessarily result in a significant increase of ultraviolet radiation reaching the ground. For the UV radiation at the ground to rise to dangerous levels, there must be a large decrease in total column ozone along the line of sight from some point on the ground to the Sun. The trajectory of the launch vehicle through the stratosphere is generally not vertical, and stratospheric wind shear disperses the plume remnant. Only if the remnant's rate of expansion is sufficient to overcome these factors is a large decrease in total column ozone possible, and in this case the expansion may lead to a dilution of the chlorine compounds in the plume to the point that the rate of ozone depletion decreases. Thus, even if it could be demonstrated that complete ozone depletion could be expected within the launch-plume remnant, there would still be questions regarding the ultimate effect on the UV flux reaching the ground.

The above discussion has concentrated on the effects of large solid-fuel rocket motors (SRM's) on the stratospheric ozone layer, because solid rockets are known to deposit large amounts of chlorine compounds in the stratosphere. The effects of smaller vehicles or liquid-fueled rockets are even more poorly known than those of SRM's. A program of remote sensing from space, such as the HIROIG program is envisioned to be, would be able to observe the effects of all the launch vehicles in the world's fleets.

### 3. The HIROIG Instrument

The HIROIG instrument is a UV hyperspectral imaging spectrograph/polarimeter. It is really three identical UV spectrographs, each fitted with a half-wave plate set at a different angle. Combining the signals from the three spectrographs allows the polarization of the incident light to be determined. Each spectrograph uses a two-dimensional charge-coupled device (CCD) as a detector. The entrance slits of the spectrographs are arranged perpendicular to the spacecraft ground track so that the slits are swept over the ground in a "push-broom" mode of observation, as illustrated in Figure 1. The image on the CCD is spatially resolved into 100 elements parallel to the spectrograph entrance slit, with the UV spectrum dispersed in the perpendicular direction. Each spectrograph simultaneously records 100 spectra divided into 100 wavelength bins in the range 270–370 nm. Spatially, the bin size is equivalent to 1 km at the Earth's surface when viewed from an altitude of 800 km, giving an effective resolution along the slit of 2 km when the instrument is pointed toward nadir. A gimbal allows the whole assembly to be pointed in the cross-track direction. Spectra are recorded every 1/7th second, which corresponds to the time for a spacecraft in Sun-synchronous orbit to travel 1 km along its ground track. Thus, the in-track resolution is approximately 2 km.

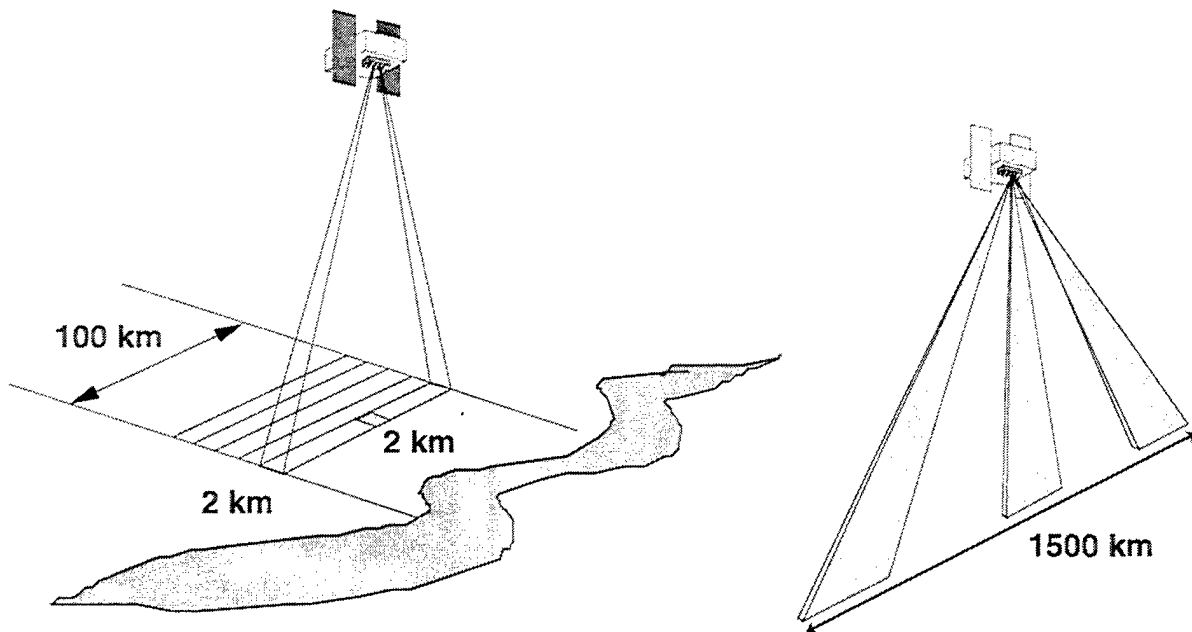


Figure 1. "Push-broom" operation of the HIROIG instrument in a Sun-synchronous polar orbit, illustrating the 100-km swath and the 2-km spatial resolution (pixel size = 1 km). The one-axis gimbal allows a cross-track field of regard of approximately 1500 km.

HIROIG will use the well-known solar UV backscatter method to search for evidence of stratospheric ozone depletion caused by launch-vehicle exhaust. This technique is used by the nation's workhorse ozone instruments, TOMS (Total Ozone Mapping Spectrometer) and SBUV (Solar Backscatter UV). Solar radiation that is incident on the upper atmosphere is absorbed by the stratospheric ozone layer and Rayleigh-scattered by gas molecules in the air. Ozone strongly absorbs in the UV, with the attenuation increasing with decreasing wavelength. The effect of a region of lower-than-normal ozone population (for simplicity of terminology, an "ozone hole") is illustrated in Figure 2. Incident light passing through the ozone hole will be able to penetrate deeper into the atmosphere, to where the atmosphere is denser. Because the atmosphere is denser, there are more scatterers, and the backscattered signal is stronger. The figure shows that light passing through an ozone hole after scattering will also be more intense since there are fewer absorbers along the exit path. Measurement of the spectrum also provides altitude information. The simplest way to understand this is to realize that short-wavelength light will not be able to penetrate deep enough into the atmosphere to be affected by an ozone hole beyond a certain depth. Thus, the signature of an ozone hole is a localized intensification of the UV spectrum, and the wavelength range in which the intensification occurs provides information about the depth at which the ozone hole is located.

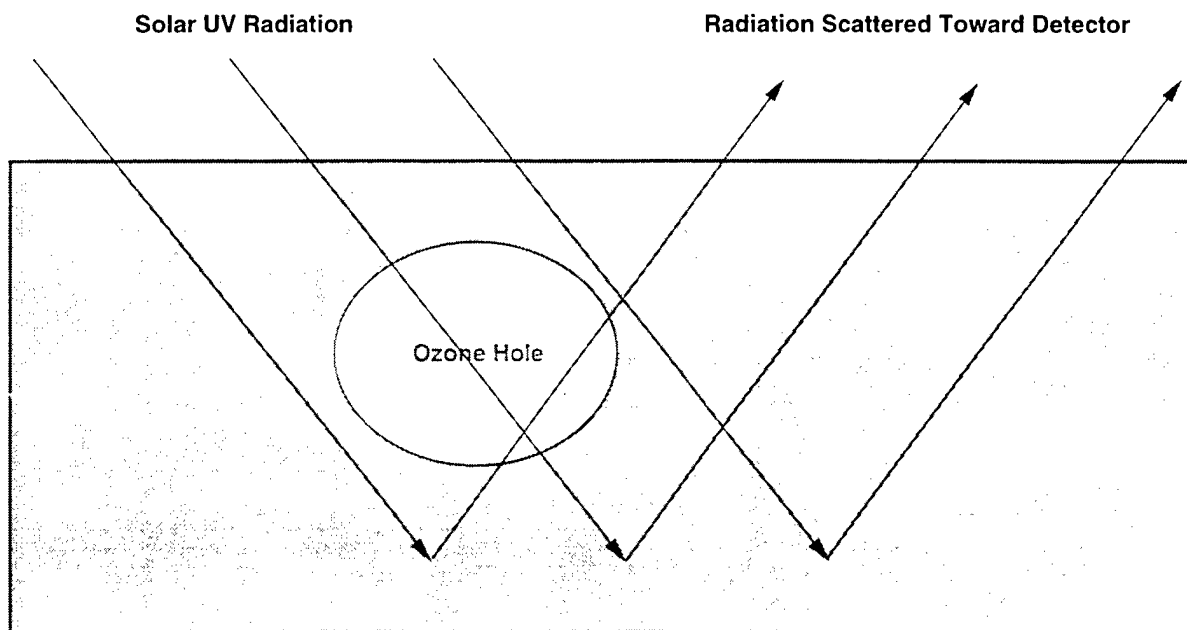


Figure 2. Illustration of the effects of an "ozone hole" on the backscattered solar UV radiation as viewed from space.

### 3.1 Optics

The optical layout of one of the three HIROIG spectrographs is shown in Figure 3. The forward cone acts as a sun shade to prevent stray light from the Sun from entering the spectrograph. Incident light is first filtered by a UV attenuator. The solar spectrum in the UV is very steep, and we must attenuate the radiation at wavelengths longer than about 310 nm in order to allow the exposure time to be long enough to measure the weaker spectrum in the ozone bands, at shorter wavelength. Following the UV attenuator is a visible-light blocker, which serves to prevent visible light from entering the spectrograph and contributing to the background counting rate; the CCD detector is sensitive to visible light.

After the light passes through the UV attenuator and the visible-light blocker it reaches the polarizing elements. A measurement of the polarization of the light is essential to the prevention of false-positive detections. We interpret a brightening in the backscattered signal as an indicator of an ozone hole. Aerosols in the launch plume can also increase the scattered-light intensity and thus may give a false indication of an ozone hole. However, the polarization of Rayleigh-scattered light is a well-known function of the Sun-scatterer-detector geometry alone and is different from the polarization of

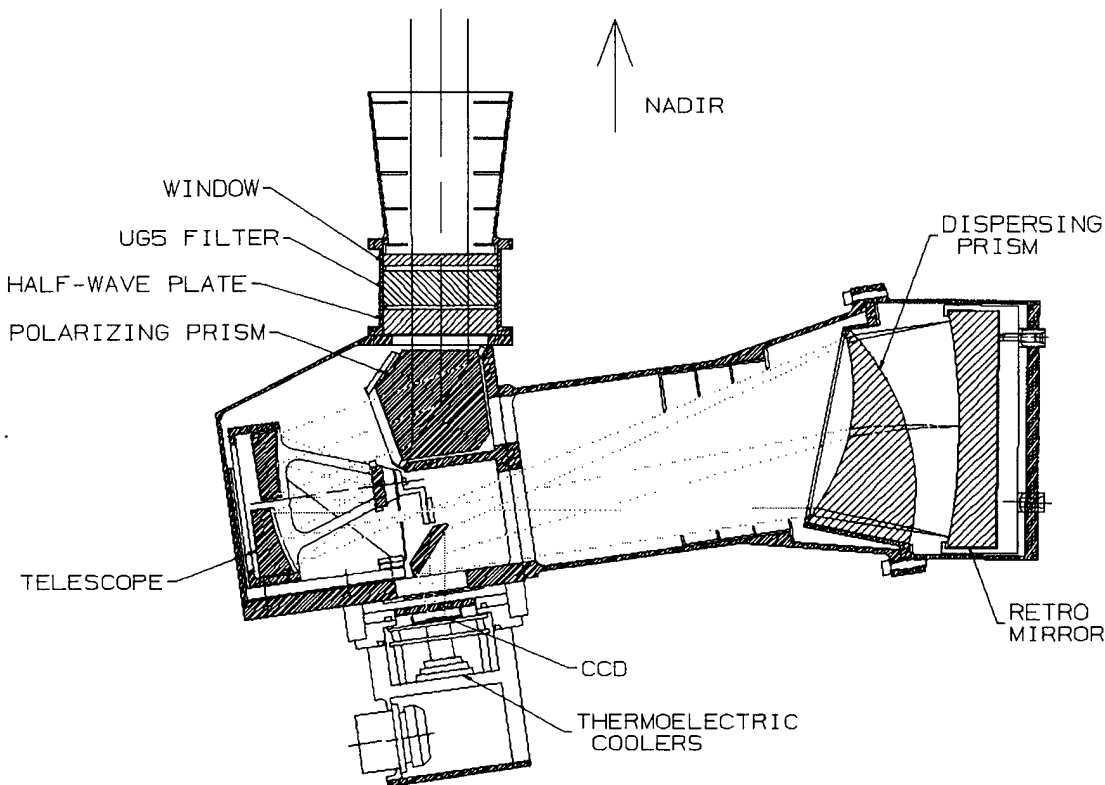


Figure 3. A cross-sectional view of one of the three identical spectrographs in the HIROIG flight instrument.

light scattered by aerosols. Thus, by measuring the polarization of the scattered light, we can eliminate false-positive detections.

The light first passes through the half-wave plate, which rotates its plane of polarization by twice the angle between the initial polarization plane and the half-wave plate's axis. The light then enters the polarizing prism, which reflects the component that is polarized perpendicular to the plane of incidence, that is, perpendicular to the plane of the figure. By orienting the half-wave plates on the three spectrographs at three different angles, we can select components of the incident light that are polarized in three different planes. This enables us to determine three of the four "Stokes parameters" that serve to give a complete description of polarized light. In simpler terms, this means that we can determine the intensity, the degree of polarization, and the plane of polarization of the incident light but not the ellipticity, which is assumed, on physical grounds, to be very close to zero. The polarizing prism also serves to reduce the polarization sensitivity of the instrument. If the angle of incidence is other than  $90^\circ$ , the reflectivity of a surface depends upon the degree and angle of polarization of the incident light. This effect is entirely eliminated for all surfaces beyond the polarizing prism, and the angle of incidence is very close to  $90^\circ$  for the upstream surfaces. Thus the polarization sensitivity of the HIROIG spectrographs is essentially zero.

Light emerging from the polarizing prism is brought to focus on the entrance slit of the spectrograph by a stigmatic three-element telescope. The spectrograph uses a prism as the dispersing element. The design is based upon that of the Broadband Array Spectrograph System (BASS; Hackwell and Warren 1992), an infrared spectrograph developed at The Aerospace Corporation. The surfaces of the prism are nonconcentric spheres. Light passes through the dispersing prism, is reflected by the rear spherical mirror, and passes through the prism a second time. The light is then reflected off the folding mirror and onto the imaging CCD detector. The spectrum is dispersed in the plane of the figure, and the image is formed parallel to the spectrograph entrance slit, perpendicular to the plane of the figure.

### 3.2 Detector

The HIROIG detector is a  $1024 \times 1024$ -element CCD; each element is  $18 \times 18 \mu\text{m}$  in size. The layout of the CCD is shown in Figure 4. The chip is divided into four segments, each  $256 \times 1024$  elements. The two center segments are exposed to the incoming light from the spectrograph. The spectral dimension is vertical, and the imaging dimension is horizontal in the figure. On-chip binning is employed to achieve the required image pixel size, corresponding to approximately 100 pixels in both the spectral and spatial dimensions. Thus, the spectrum in the wavelength range of 270–370 nm is divided (nonlinearly) into 100 bins, and the 100 spatial pixels give a pixel size of 1 km at nadir when the Earth is viewed from a Sun-synchronous altitude of approximately 800 km. The two outer segments of the CCD are used as parallel storage registers and are masked to prevent illumination by stray light.

The desirability of segmenting the CCD as shown can be understood by referring to the raw spectrum shown in Figure 5. In the figure, the CCD signal strength is plotted as a function of wavelength in nanometers for a scattered-light spectrum measured from the ground at Cape Canaveral at 13:20 EDT on July 7, 1997. At this time, the solar zenith angle was approximately  $6^\circ$ , and the spectrograph was pointed  $9^\circ$  from the zenith and  $15^\circ$  from the Sun. The measured spectrum in Figure 5 is primarily

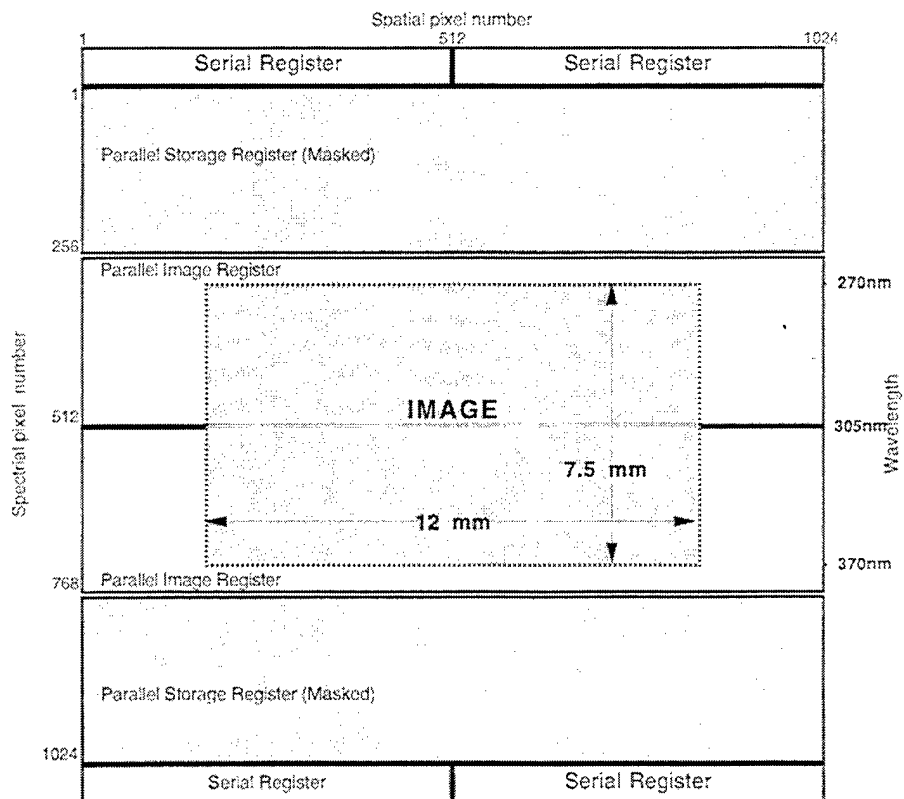


Figure 4. Layout of the 1024 X 1024-pixel HIROIG CCD detectors. The two center segments are used for imaging, and the two outer segments for storage and transfer of the image.

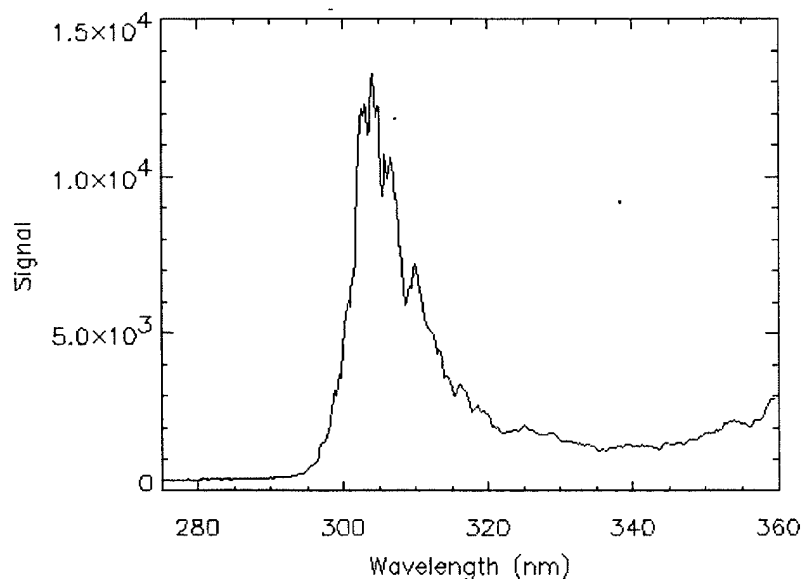


Figure 5. The UV spectrum of the diffuse sky as recorded by the HIROIG prototype instrument at Kennedy Space Center on July 7, 1994 at 13:20 EDT, when the Sun was near the zenith.

shaped by the steep fall-off of the solar UV spectrum with decreasing wavelength, the UV attenuator in the HIROIG instrument (at wavelengths above 300 nm), and atmospheric ozone absorption. The main difference between this spectrum and the backscattered spectrum measured from space is that the ground-based spectrum has no detectable signal below approximately 290 nm, while the space-based spectrum would be detectable down to the lowest HIROIG wavelength of 270 nm. The spectrum peaks at 305 nm, which corresponds to the center of the CCD (see Figure 4). The CCD is read out by a series of parallel shifts of the charge in the bins to adjacent bins, like a "bucket brigade," from the center outward. Because the instrument has no shutter, the detector continues to collect charge during the rapid parallel shift-out of the image. By shifting out the brightest part of the spectrum last, we assure that the distortion of the spectrum due to the small amount of charge collected during the parallel shifting is negligible. In addition, with each shift, a very small amount of charge is left behind, and the accumulation of that charge after a large number of shifts can result in an enhanced signal in the trailing pixels. If dim parts of the spectrum are shifted out after bright parts, a distortion of the spectrum can result that is not negligible. By assuring that the brightest part of the spectrum is shifted out last, we minimize this effect.

The modes of the CCD are shown schematically in Figure 6; the four segments are denoted as Pe...Ph. The first step involves only the center two segments, in which the image is made. If necessary, a few shifts center the image so that the on-chip binning will result in wavelength bins with wavelength intervals that do not change over time. The amount of shift required is determined by occasional wavelength-calibration runs. In the second step, the frame transfer from the imaging segments to the storage segments is made. This erases the imaging segments, except for the small amount of charge

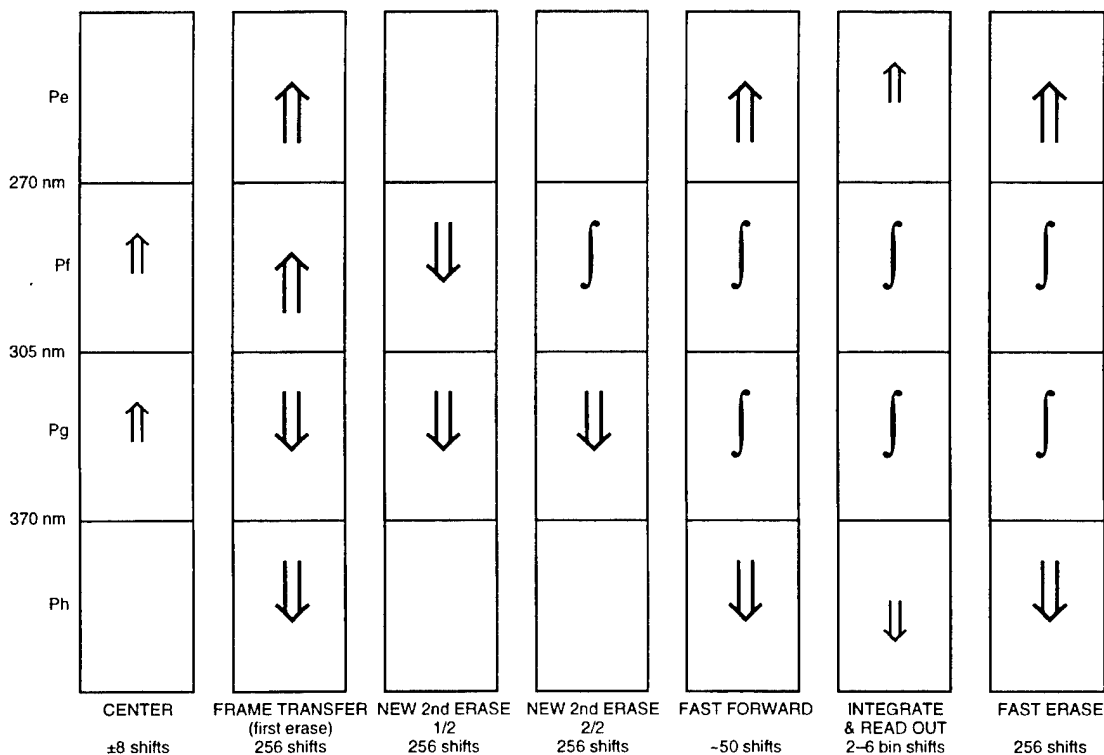


Figure 6. Illustration of the modes of operation of the parallel registers of the HIROIG CCD detector.

left behind because of imperfect charge transfer efficiency. In the next two steps, the imaging segments are erased again. Since the CCD has no shutter, and the center segments are always exposed to the incoming radiation, image accumulation in a given bin begins as soon as the second erase for that bin occurs. The time required for a single parallel shift is somewhat less than  $3\ \mu\text{s}$ , so the total accumulation time at the shortest wavelength is approximately 1.2 ms longer than that at the longest wavelength; the imaging cadence for the spaceborne instrument is 143 ms per image. The "fast-forward" shifts in the next step throw away the part of the image that lies outside the specified HIROIG wavelength range. The next step is the read out of the image from the storage registers while the new image is being accumulated. On-chip binning is accomplished by making 2–6 parallel shifts into the four output registers and then shifting out the image serially and repeating the process until the entire image is read out. Finally, the storage registers are quickly erased, and the process starts over.

The detector electronics block diagram is shown in Figure 7; details are shown for one of the three spectrographs. The operation of the detector is controlled by a microsequencer with its program stored in random-access memory (RAM). The four serial registers transfer the data to preamplifiers

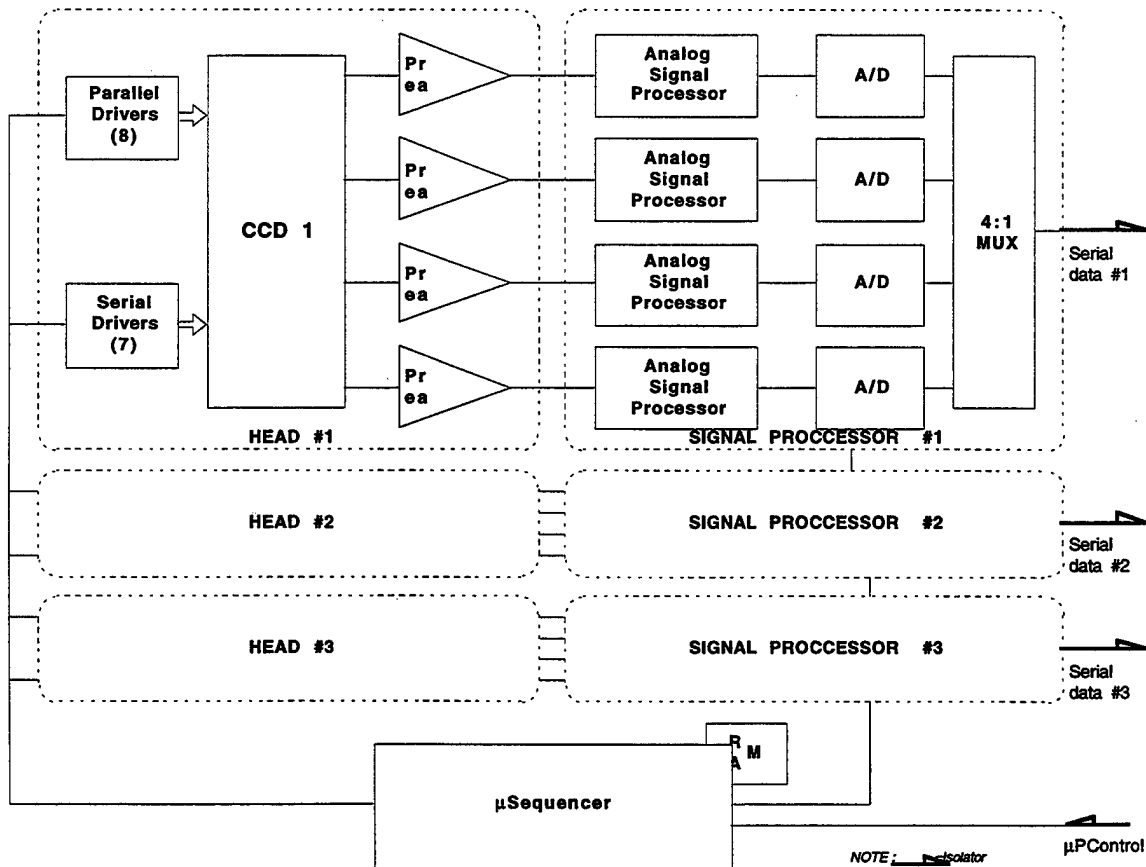


Figure 7. Block diagram of the HIROIG CCD detector electronics.



that are close to the chip. The analog signal processors, analog-to-digital converters, and a multiplexer for each of the spectrographs are in a separate box that is near the detector head. The multiplexer combines the data that originates from the four serial outputs of the chip into one serial data stream that is directed to the data processing unit.

### 3.3 Data Processing Unit

HIROIG has a high data-taking rate, which is the main factor in levying requirements on the data processing unit (DPU). During data acquisition following a launch, each of three spectrographs produces a 100 x 100-pixel image seven times per second. Since the signal from each pixel is compressed into one 8-bit byte, the total data rate is  $100 \times 100 \times 3 \times 7 \times 8 = 1.68 \times 10^6$  bit/s. An observing sequence for a launch would typically require recording upwards of 40 Mbytes of data. In addition, the DPU must exercise a number of control functions. The requirements can be summarized as follows.

- Record 1.68 Mbit/s
- Provide 64 Mbyte of single-event-effect-immune image-data storage
- Time-tag, compress, and packetize image data for spacecraft delivery
- Digitize and monitor housekeeping data
- Provide multiple-detector readout microsequencer "programs"
- Process ground commands for pointing and data accumulation control
- Initialize and stabilize detectors and gimbal before data acquisition
- Provide for calibration mode operation
- Provide thermal control and safeguarding as necessary

The Aerospace Corporation's Space and Environment Technology Center is developing a "modular DPU" for a number of spaceflight programs; including HIROIG. The modular DPU has a common packaging scheme and quasi-standard electronic circuit boards, and can include space for application-specific circuit boards. Application-specific boards in the HIROIG DPU perform data recording (4 boards) and provide an interface to the thermal control and gimbal systems (1 board). A block diagram of the HIROIG DPU, with eight circuit boards, is presented in Figure 8. Four of the eight boards comprise the 64-Mbyte solid-state data recorder system. The DPU can ingest high-rate data, process it, and then transfer it to the spacecraft telemetry system at any specified rate. An average continuous spacecraft data rate for HIROIG as low as 10 kbit/s is acceptable. At this rate, the 42 Mbytes of data for a typical postlaunch observation could be read out to spacecraft telemetry in 9 h 20 min. This is acceptable because a given launch site would be in view of HIROIG aboard a low-Earth-orbit spacecraft and in sunlight only once per day. In practice, the read-out time could be reduced by a factor of 2–2.5 through data compression operations carried out in the DPU.

# DPU BLOCK DIAGRAM (8 BOARDS; POWER DISTRIBUTION NOT SHOWN)

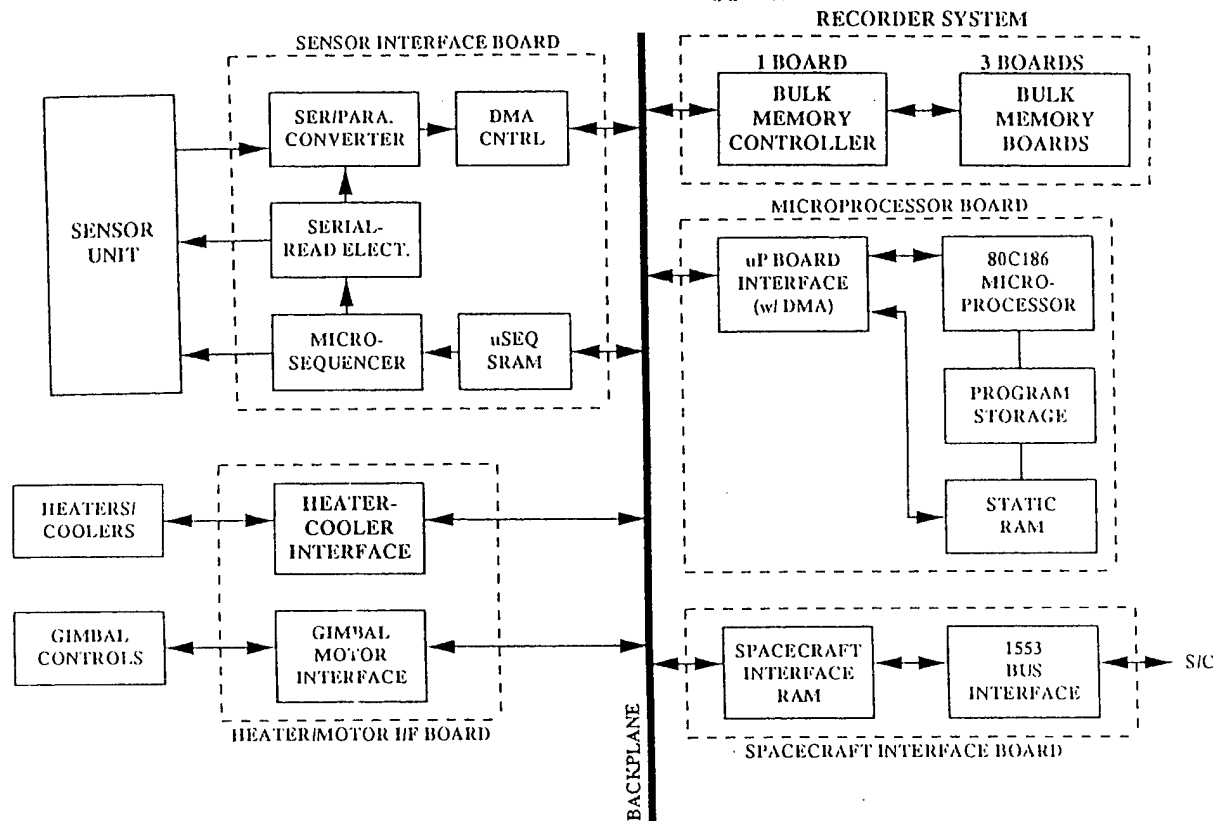


Figure 8. Block diagram of the HIROIG data processing unit.

The heart of the DPU is the microprocessor board, which controls the instrument operation. The instrument has the following four modes of operation:

**Maintenance Mode.** In this mode, the parameters are set for an upcoming data acquisition. Ground commands provide gimbal pointing instructions and the start time and duration of the data take. The latest calibration data are acquired; this information is used to program the spectrum-centering shifts prior to CCD data transfer.

**Set-up Mode.** Various control functions prior to the data take are exercised. If the thermoelectric coolers on the detectors are not already in operation, they are activated, allowing adequate time before the data-acquisition sequence for detector cooling and temperature stabilization. The gimbals are pointed and the data recorder partitioning into three segments (partitions 0, 1, and 2) is initialized. The microprocessor then awaits the ground-commanded acquisition start time and then transfers into the data acquisition mode.

**Data Acquisition Mode.** The microsequencer program and hardware control the CCD fast frame transfer, data read-out and digitization, and serial read-out to the DPU sensor-interface board. During the CCD fast frame transfer, the microprocessor puts header information out to the data recorder for the next set of images, monitors the analog housekeeping data, and decrements the number of images required to complete the observing sequence. When the data take is complete or the data recorder is full, the microprocessor enters the compression/read-out mode.

**Compression/Read-out Mode.** As the name implies, in this mode, the data are compressed and read out to the spacecraft telemetry system. The data compression operations can be overridden by ground command. Partition 0 of the data recorder is used to read the next image to be processed into the static RAM on the microprocessor board. A lossless data compression algorithm is performed in the static RAM, and the compressed data are rewritten to partition 1. The read-out operation transfers data to partition 2 for telemetry output. When the read-out is complete, the microprocessor is returned to the maintenance mode.

Figure 9 is a block diagram of the solid-state data recorder. In addition to its memory-control functions, the memory controller performs error detection and correction (EDAC). To each 32 bits of raw data, an 8-bit Hamming code is added; the resulting 40 bits are stored in bulk memory (25% EDAC overhead). Periodic memory read/rewrite is performed under microprocessor control. A commercial bulk memory chip was selected to minimize cost and availability difficulties. The memory design provides for graceful degradation and mitigation of single-point failures. The chips are immune to latch-up and are radiation-hardened to 30 krad total dose, more than adequate for the desired HIROIG

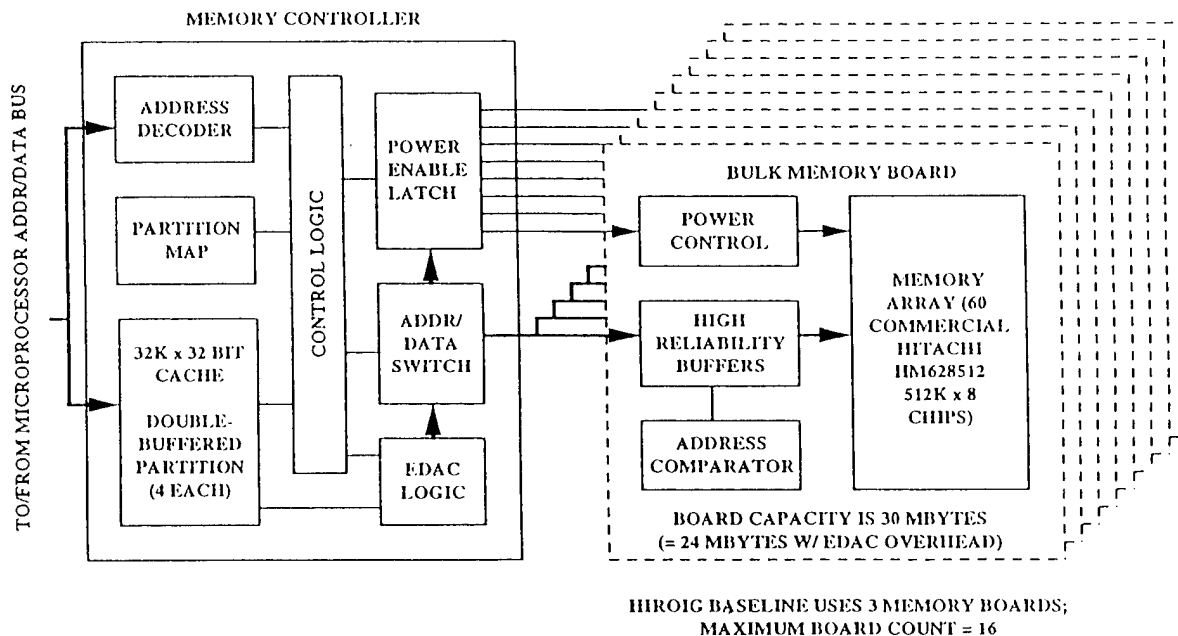


Figure 9. Block diagram of the HIROIG solid-state data recorder.

orbit and a 3-year lifetime. Although single-event upsets will occur, the memory controller will correct for single-event effects. HIROIG uses three bulk memory boards, each of which has a standard capacity of 30 Mbyte, enough for 24 Mbyte of data with a 6-Mbyte EDAC overhead. The recorder meets the standard for storage of 64 Mbyte of raw data, with adequate capacity for the data compression and telemetry read-out partitions.

### **3.4 Calibration**

The HIROIG instrument requires two forms of calibration: wavelength calibration and intercalibration of the responses of the three spectrographs. Since HIROIG searches for changes in the backscattered solar UV spectrum caused by ozone depletion in small regions, an absolute calibration, which is essential for monitoring long-term trends in the global stratospheric ozone layer, is not needed by HIROIG. Nevertheless, it is desirable to have an absolute calibration, which can be obtained by comparison with TOMS data. Up-to-date wavelength calibration is needed primarily to assure that the on-chip binning is always performed in a consistent way. Wavelength calibration data for all three spectrographs must be provided to the instrument before the observation set-up operations can be performed. An accurate determination of the polarization of the backscattered sunlight is crucial for the primary HIROIG mission, the search for ozone depletion caused by launch vehicle exhaust. Since polarization is determined by comparing the spectra measured by all three spectrographs, intercalibration of the spectrograph responses is essential.

Obtaining the wavelength calibration requires using the full resolution capabilities of the spectrographs; these are degraded by on-chip binning in the normal data acquisition mode of operations. The time to acquire a single spectrum can be increased to maintain good counting statistics. Two techniques are available. One is to use a standard atomic calibration lamp to illuminate each spectrograph during a calibration run. An alternative is to rely upon features in the backscattered solar radiation spectrum; Figure 5 shows several such features at the full spectral resolution of the ground-based HIROIG prototype instrument. The baseline is to use the latter method because it is instrumentally simpler. Whichever method is used, ground-based analysis of calibration spectra is required prior to any data take. The results can then be uplinked and used to set up the control of the CCDs during the observation.

There are two requirements for spectrograph intercalibration. The first is to determine the relative response of the spectrographs to identical backscattered solar UV spectra. The second is to determine the relative pointing of the spectrographs to an accuracy of 1–2 arc minutes; the HIROIG image pixel size is 4.3 arc minutes. Initial coalignment of the spectrographs to this accuracy should not be difficult, but monitoring is necessary because shifts might occur when the spacecraft carrying HIROIG is launched, or due to the on-orbit thermal environment.

Determination of the relative response of the spectrographs can be made using backscattered solar radiation spectra. Since the spectrographs each include a polarizing prism, they respond differently to polarized light; therefore, the intercalibration must be done with unpolarized light. The degree of polarization of backscattered solar radiation is:

$$P = \frac{\sin^2 \theta}{1 + \cos^2 \theta}, \quad (3)$$

where  $\theta$  is the scattering angle. For  $|\theta - 180^\circ| < 4^\circ$ ,  $P$  is less than 0.25%, which we take as an upper limit on the tolerable polarization of the light that is incident on the HIROIG sensor during a calibration sequence. By gimbaling across-track, HIROIG will be able to view light satisfying the above polarization condition for approximately 15 s per orbit, provided that HIROIG is able to view directly backscattered radiation at all. This is adequate time to obtain over 100 spectral images for each spectrograph and thus a good calibration of the spectrographs' relative sensitivity. The requirement to be able to view backscattered radiation places limits on the range of acceptable orbits, given that the instrument can only point cross-track by  $45^\circ$ . For Sun-synchronous orbits, which are most desirable for HIROIG, the local time of the ascending or descending node must be between 08:46 and 15:14. If the orbit is not Sun-synchronous, this calibration will be unavailable whenever the angle between the orbit plane and the incident sunlight exceeds approximately  $48.6^\circ$  ( $45^\circ$  cross-track pointing plus instantaneous cross-track field of view of  $\pm 3.6^\circ$ ).

The strategy for monitoring the spectrograph coalignment is to image, at the highest resolution available, terrestrial features for which the UV albedo undergoes a rapid change. The edge of a cloud or glacier could be such a feature. The time-dependent signals in the longest-wavelength channels of the three spectrographs would be compared to establish the coalignment.

### 3.5 Electronic Ground Support Equipment

The HIROIG electronic ground support equipment (EGSE) is being developed in three phases: sensor development, DPU check-out support, and full HIROIG system check-out support. The EGSE is based upon a Macintosh computer. In the sensor development phase, we are concerned with handling data that are acquired directly from the three sensor heads. Means and standard deviations are calculated, row and column histograms are displayed, and data are archived through an interface to the Microsoft Excel spreadsheet application. In the DPU check-out support phase, the EGSE performs the following functions, using simulators for the instrument and spacecraft systems: closed-loop testing of gimbals and heaters; verification of command operation; closed-loop testing of the conversion of simulator data to spacecraft data for validation of the data-compression algorithms in the DPU; overcurrent protection of the spacecraft power simulator; raw data archival and display; and housekeeping data archival and display. The HIROIG team has gained extensive experience in collecting, processing, displaying, and archiving CCD image data through our work with the prototype instrument. The software developed for that instrument was based on that used with pre-existing and ongoing ground-based observation programs that used CCD-based imagers. Thus, we have powerful CCD imaging software that can be used as a basis for performing image display and making three-dimensional surface plots of ozone maps during the full-system check-out phase of the program. The software includes a built-in image calculator. Additional functions that will be performed by the EGSE during this phase are safeguarding the sensor and the DPU by limit checking on temperature, current, and voltage; simulation of spacecraft commands; and archival and playback of telemetry data.

#### 4. HIROIG Instrument Development Status

The status of the HIROIG instrument development as of the end of FY97 can be summarized as follows. All of the mechanical parts for the three spectrographs have been made, and one of the new spectrographs (the "old" spectrograph is the prototype, which has been used for ground-based observations for several years) was assembled for a fit check and then disassembled. The optics are also complete except for coating of one polarizing prism and construction of two roof prisms for the polarizing prisms in the new spectrographs. Applying the coating is a specialized job done by an outside vendor, but the roof prisms can be made in the Aerospace shop. When the last of the optics are in hand and the interior surfaces of the housings are painted flat black, the spectrographs will be ready for final assembly.

The one major part of the design that remains outstanding is the detector and its electronics. While we have demonstrated operation of an engineering-grade detector in the high-speed, high-resolution mode needed for the spaceflight instrument, the flight-quality detectors have not yet been tested. A number of detailed design issues depend on the work with the flight detectors, and some of these, such as packaging, cooling, and radiation shielding have important bearing on the final mechanical design of the instrument.

Most of the circuit boards in the DPU have been designed and are in the prototype/test phase of development. Exceptions are the MIL-STD-1553 spacecraft interface board and the sensor interface board, both of which are partially completed but require further design work. The power converter boards that provide power to the DPU and to the detectors' thermoelectric coolers are conceptually designed and are awaiting establishment of the final instrument power requirements of both subsystems. A commercial line of power supplies has been identified for use. The solid-state memory uses a commercial chip with a design that provides for graceful degradation and single-point failure mitigation rather than an expensive high-reliability chip with a long purchasing lead time. This makes it possible to build up flight memory boards at an early stage. The selected chip is immune to latch-up and is hardened to a total dose of 30 krad, which is adequate for the desired HIROIG orbit. The chip will experience single-event upsets, but their effects will be corrected by the memory controller. The other boards, besides the bulk memory, will use high-reliability parts. For these, flight versions will be built up when and if a flight has been identified for the instrument. Finally, the detailed mechanical design of the DPU box is finished.

There are a few items that depend upon interface information that is not available to us in advance of a flight assignment for the instrument. We have not designed these items in any detail because it would be premature to do so. An obvious example is the spacecraft interface electronics. For purposes of testing, we have incorporated a MIL-STD-1553 spacecraft interface, which is a plausible but not certain choice, into the DPU. Similarly, the gimbal system may be constrained by spacecraft mechanical interface specifications, and so it has only been carried along as a concept. We do not anticipate any problem in designing the gimbal; it has motion about a single axis and essentially no minimum-speed requirement. Finally, we have not done any design of an on-board calibration system. Our baseline is to use the backscattered solar spectrum for both wavelength-calibration and determination of the relative sensitivities of the three spectrographs. This is very likely to be the best approach, but HIROIG could be offered a flight aboard a spacecraft having an orbit that is acceptable

for making the observations we wish to make, but for which the full calibration cannot be performed without using built-in lamps. In that case, an on-board calibration system would have to be developed. Our team has extensive experience with UV calibration lamps, and we see no problem in implementing on-board calibration if it is needed.

## 5. Ground-Based Observations

A number of ground-based observation programs have been carried out with the HIROIG prototype sensor. These programs have had several goals: initial system check-out and calibration, assessment of the performance and sensitivity of the spectrographs, and collection of scientifically or technologically valuable data. Two of these observation programs are especially important to the HIROIG program. Observations carried out at the Kennedy Space Center (KSC) in Florida associated with the space shuttle STS-65 launch demonstrated the instrument's ability to detect evidence of local ozone depletion, and observations of noctilucent clouds carried out at Søndre Strømfjord, Greenland in July 1995 demonstrated the instrument's high sensitivity and the usefulness of its polarimetry function.

In May 1994, we were offered an opportunity to use the HIROIG instrument to make ground-based observations in conjunction with the launch of the STS-65 space shuttle mission. The launch trajectory was to be due east with a launch time around local noon on July 8, just after summer solstice. At this time of the year, the stratospheric winds blow predominantly toward the west, so the launch plume remnant would be advected back over the launch pad. It even seemed likely that the stratospheric wind shear would result in a vertical "stacking-up" of the plume as it moved to the west over available observing sites on KSC. In short, this launch seemed to be an ideal opportunity to search for evidence of ozone depletion caused by solid rocket motor exhaust. Therefore, we agreed to carry out an observing campaign on July 7-9 at KSC. There was some risk involved in this since we had not previously contemplated making this type of observation. In fact, the data taken on July 7 and July 9 were compromised to some extent because of the unanticipated effects of the high summer humidity in Florida on the instrument, but the data taken on July 8, the launch day, were completely unaffected.

Observations of the diffuse scattered solar UV spectrum of the sky were made from a site 6.4 km due west of the STS-65 launch pad. The instrument was pointed in three directions, near zenith, south of zenith, and north of zenith, all in a plane containing the zenith, the Sun, and (of course) the instrument. For each pointing direction, three exposures, with different settings of the HIROIG half-wave plate, were made. The three exposures selected light that was linearly polarized in the "scattering plane" described above, perpendicular to the scattering plane, and at an angle of  $45^\circ$  to the scattering plane. Each exposure sequence consisted of 10 exposures, three for each of the pointing directions and one dark exposure with the shutter closed. Each exposure produced an image with 204 columns (spatial dimension) by 512 rows (spectral dimension). Images selecting polarization parallel and perpendicular to the scattering plane were summed to obtain an intensity image (the I Stokes parameter). Spectra such as that in Figure 5 were obtained by summing over 10 columns in the spatial direction. These spectra were used in the analysis.

The results of the analysis of the STS-65 launch-day (July 8, 1994) data are summarized in Figure 10. It plots the ratio of UV radiation detected by HIROIG in two wavelength bands centered on 299.9 nm (numerator) and 297.7 nm (denominator) as a function of time. Two minimum- $\chi^2$  fits to the data are shown. The quadratic fit is of the form



$$R = at^2 + b, \quad (4)$$

while the zenith fit is of the form

$$\ln(R) = a[\sec(\zeta(t))] + b, \quad (5)$$

where  $\zeta(t)$  is the solar zenith angle as a function of time. The zenith fit is the behavior that would be expected if all of the ozone in the atmosphere were concentrated in a planar layer having no temporal or spatial variations. Each data point in the figure is the sum of data from nine spectra like that in Figure 5, three spatial slices from the intensity image at each of three instrument pointings. The error bars are  $\pm 1\sigma$ . For 10 min, starting at about 13:00 EDT, the data deviate from the fits by as much as  $-2.0\%$ . This deviation is small but highly significant, as can be seen from the error bars. A local decrease in the total ozone column by 2.35% could account for the observed sudden change in the intensity ratio plotted in Figure 10. An alternative explanation, wavelength-dependent scattering effects, has been eliminated by the observation that the spectrum outside the strongest ozone absorption bands did not show similar effects.

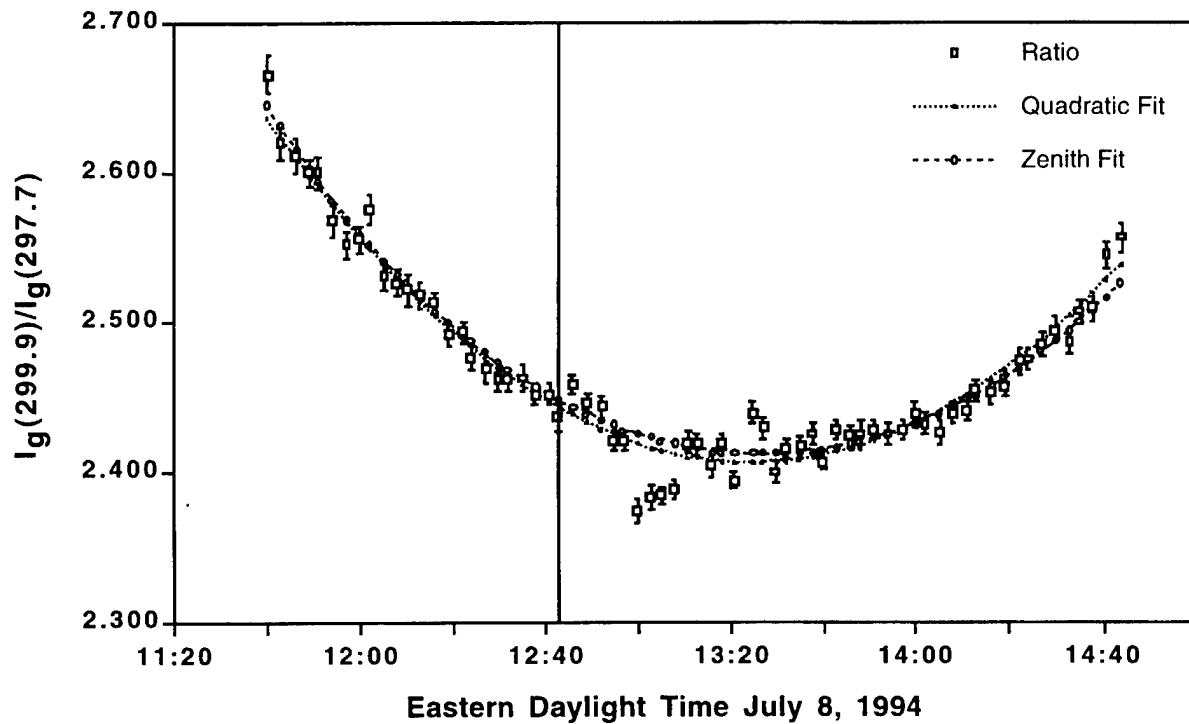


Figure 10. Plot of the intensity ratio of diffuse sky radiation in bands centered on 299.9 nm and 297.7 nm as a function of time on July 8, 1994. The data were taken from a site 6.4 km due west of the launch pad for the STS-65 space shuttle flight. The vertical line indicates the launch time, 12:43 EDT.

The suggestion that the change in the ratio plotted in Figure 10 was caused by stratospheric ozone depletion associated with the STS-65 launch plume was tested with a simple empirical model of plume transport and growth. The "stratosphere" gets its name from the high degree of stratification of the atmosphere in this region. Therefore, we assumed that plume segments in thin layers would grow and be transported by winds independently of one another and with no mixing between layers. For convenience, we assumed a layer thickness of 305 m, which corresponds to the sampling interval for the rawinsonde that provided a launch-site wind profile 30 min before launch. The location of the plume slice as a function of time was based on the prelaunch wind profile and the launch trajectory. Each segment was assumed to expand radially according to

$$r(h) = 0.05 + 0.07[t - t_0(h)], \quad (6)$$

where  $t_0(h)$  is the time (in minutes) at which the launch vehicle was at altitude  $h$ , and  $r(h)$  is expressed in km. This relation is based on a lidar measurement reported by Dao *et al.* (1997). A standard model of ozone mixing ratio versus height is used, and the ozone within each disk-shaped segment is assumed to be 35% depleted. Using these data, we can calculate the column ozone at any time, as the plume segments drift through the line of sight between HIROIG and the Sun. In Figure 11, the model calculations are compared with the total column ozone depletion inferred from the data in Figure 10. The agreement shown in Figure 11 is good and bolsters our conclusion that a small amount of local ozone depletion occurred following the STS-65 launch. That the total column ozone depletion was

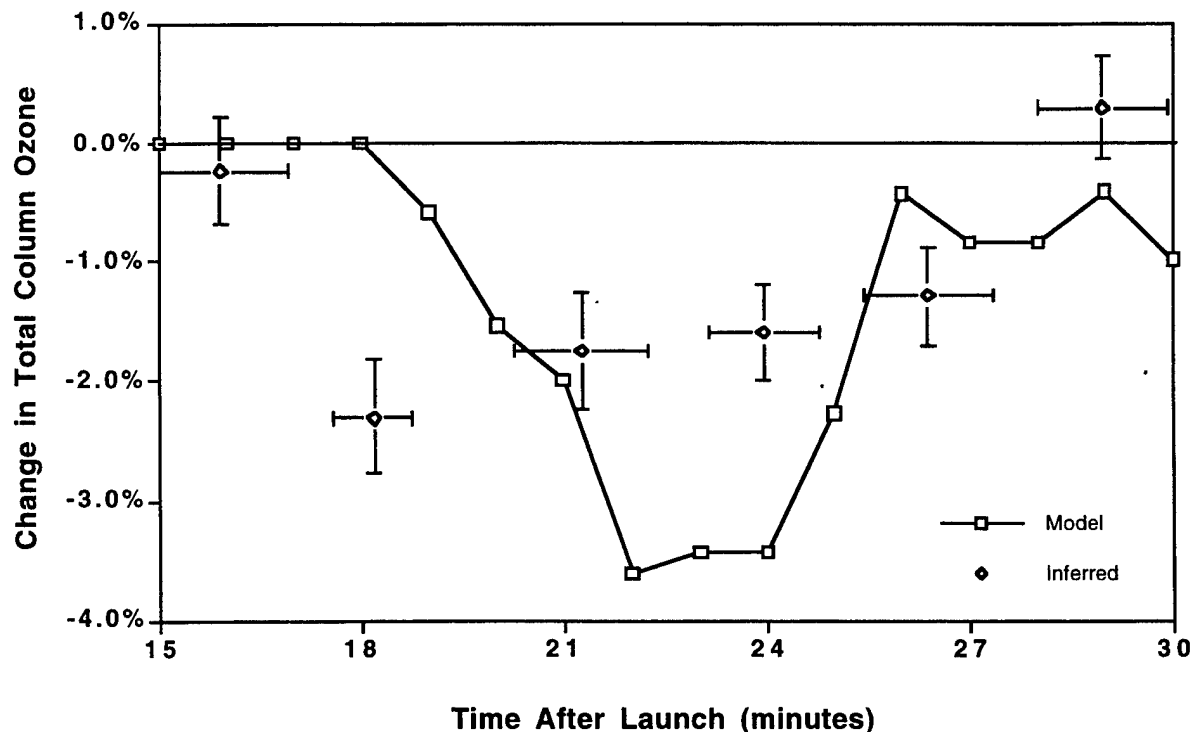


Figure 11. Comparison of the change in total column ozone inferred from the HIROIG UV spectra with that predicted by an empirical model, for July 8, 1994, following the STS-65 launch

small compared to the assumed degree of depletion in each plume segment is attributed to dispersion of the plume by stratospheric wind shear.

Ground-based observations of noctilucent clouds (NLCs) at Søndre Strømfjord, Greenland, sponsored by the Aerospace Sponsored Research and Independent Research and Development (IR&D) programs, with National Science Foundation participation, are important as a demonstration of HIROIG's capabilities. NLCs occur only in the arctic summer and, at 85 km, are the highest clouds known. Because they are far above the ozone layer, they are not observable from the ground in the ozone absorption bands but only in the long-wavelength part of the HIROIG spectral range. They are very faint and, in the UV, can only be seen in scattered sunlight after ground-level sunset, when the Earth and the lower atmosphere are not directly illuminated by the Sun. Even then the NLC signal-to-background ratio is 0.01–0.1. HIROIG has detected NLCs on the nights of July 30/31, 1995 and July 29/30 and August 4/5, 1997. The analysis of the 1995 observation is complete (Hecht, *et al.* 1997). The major scientific result of this analysis is an upper limit of 0.07  $\mu\text{m}$  on the size of the particles in an NLC. To derive this result, it was necessary to determine the polarization of the scattered light in wavelength bands centered at 330 and 375 nm. Bearing in mind the low signal-to-background ratio, the ability to obtain this result is strong testimony to the sensitivity of HIROIG. In addition it is a demonstration of the polarimetry capability of the instrument and its utility.

## 6. Summary

The HIROIG instrument was conceived to provide data on the effects of launch-vehicle exhaust on the stratospheric ozone layer. The information is required to enable the Air Force to comply with the National Environmental Policy Act, which requires government agencies to make a diligent effort to assess the impacts of their programs on the environment and to report the results of the assessment to the public. The instrument is a hyperspectral imaging spectrograph/polarimeter that measures the spectrum of solar UV radiation backscattered by the Earth's atmosphere with a spatial resolution of approximately 2 km at nadir. High spatial resolution is required because regions of ozone depletion caused by launch-vehicle exhaust are expected to be only a few kilometers in size. Since ozone absorbs UV radiation, the signature of a region of ozone depletion is an increase in backscattered radiation, and the wavelength range in which the increase occurs is indicative of the altitude at which the ozone has been destroyed. HIROIG's capability for characterizing the polarization of the incident radiation allows it to avoid false-positive signals that might arise as solar radiation is scattered by aerosols in the launch-plume remnant. Thus, the instrument has a unique combination of capabilities in several areas in order to be able to perform its mission of obtaining unambiguous information regarding the prompt local effects of space launches on stratospheric ozone. These capabilities have been demonstrated by a series of tests and observations of the atmosphere made with a prototype spectrograph.

## References

- Brady, B. B. and L. R. Martin, "Modeling Solid Rocket Booster Exhaust Plumes in the Stratosphere with Surface Chemkin," TR-95(5231)-9, The Aerospace Corporation, El Segundo, CA, 1995.
- Dao, P. D., J. A. Gelbwachs, R. Farley, R. Garner, P. Soletsky, and G. Davidson, "LIDAR Stratospheric SRM Exhaust Plume Measurements," AIAA 35th Aerospace Sciences Meeting, Paper 97-0526 (1997).
- Denison, M. R., J. J. Lamb, W. D. Bjorndahl, E. Y. Young, and P. D. Lohn, *J. Spacecr. Rockets* **31**, 435 (1994).
- Hackwell, J. A. and D. W. Warren, *Proc. SPIE* **1745**, 290 (1992).
- Hecht, J. H., J. P. Thayer, D. J. Gutierrez, and D. L. McKenzie, "Multi-instrument Zenith Observations of Noctilucent Clouds over Greenland on July 30/31, 1995," *J. Geophys. Res.* **102**, 1959-1970 (1997).
- L. R. Martin, "Possible Effect of the Chlorine Oxide Dimer in Transient O<sub>3</sub> Loss in Rocket Plumes," TR-94(4231)-1, The Aerospace Corporation, El Segundo, CA, 1994.
- Ross, Martin, *J. Spacecr. Rockets* **33**, 144 (1996).
- Ross, M. N., J. R. Benbrook, W. R. Sheldon, P. F. Zittel, and D. L. McKenzie, "Observation of Stratospheric Ozone Depletion in Rocket Exhaust Plumes," *Nature* (accepted for publication).
- Zittel, P. F., "Computer Model Calculations of the Local Effects of Large Solid Fuel Rocket Motors on Stratospheric Ozone," TR-94(4321)-19, The Aerospace Corporation, El Segundo, CA (1994).

## TECHNOLOGY OPERATIONS

The Aerospace Corporation functions as an "architect-engineer" for national security programs, specializing in advanced military space systems. The Corporation's Technology Operations supports the effective and timely development and operation of national security systems through scientific research and the application of advanced technology. Vital to the success of the Corporation is the technical staff's wide-ranging expertise and its ability to stay abreast of new technological developments and program support issues associated with rapidly evolving space systems. Contributing capabilities are provided by these individual Technology Centers:

**Electronics Technology Center:** Microelectronics, VLSI reliability, failure analysis, solid-state device physics, compound semiconductors, radiation effects, infrared and CCD detector devices, Micro-Electro-Mechanical Systems (MEMS), and data storage and display technologies; lasers and electro-optics, solid state laser design, micro-optics, optical communications, and fiber optic sensors; atomic frequency standards, applied laser spectroscopy, laser chemistry, atmospheric propagation and beam control, LIDAR/LADAR remote sensing; solar cell and array testing and evaluation, battery electrochemistry, battery testing and evaluation.

**Mechanics and Materials Technology Center:** Evaluation and characterization of new materials: metals, alloys, ceramics, polymers and composites; development and analysis of advanced materials processing and deposition techniques; nondestructive evaluation, component failure analysis and reliability; fracture mechanics and stress corrosion; analysis and evaluation of materials at cryogenic and elevated temperatures; launch vehicle fluid mechanics, heat transfer and flight dynamics; aerothermodynamics; chemical and electric propulsion; environmental chemistry; combustion processes; spacecraft structural mechanics, space environment effects on materials, hardening and vulnerability assessment; contamination, thermal and structural control; lubrication and surface phenomena; microengineering technology and microinstrument development.

**Space and Environment Technology Center:** Magnetospheric, auroral and cosmic ray physics, wave-particle interactions, magnetospheric plasma waves; atmospheric and ionospheric physics, density and composition of the upper atmosphere, remote sensing, hyperspectral imagery; solar physics, infrared astronomy, infrared signature analysis; effects of solar activity, magnetic storms and nuclear explosions on the earth's atmosphere, ionosphere and magnetosphere; effects of electromagnetic and particulate radiations on space systems; component testing, space instrumentation; environmental monitoring, trace detection; atmospheric chemical reactions, atmospheric optics, light scattering, state-specific chemical reactions and radiative signatures of missile plumes, and sensor out-of-field-of-view rejection.